Vibrational Properties and Structure of Pentaerythritol Tetranitrate

Yuri A. Gruzdkov and Yogendra M. Gupta*

Institute for Shock Physics and Department of Physics, Washington State University, Pullman, Washington 99164-2816

Received: December 7, 2000; In Final Form: March 16, 2001

Geometry optimizations and normal-mode analyses of the pentaerythritol tetranitrate (PETN) conformer belonging to the S_4 molecular point group and comprising the crystalline solid were performed using density functional theory methods (B3LYP and B3PW91). The basis sets used in this study were 6-31G(d) and 6-311+G(d,p). The structural results are in good agreement with experimental X-ray diffraction data. The predicted bond lengths and bond angles are accurate to within ∼2.5% and ∼1.2%, respectively. Raman and infrared spectra of crystalline PETN were measured and compared with the calculated spectra. The calculated and measured spectra agree very well in the spectral region below 1100 cm^{-1}; the agreement is satisfactory for frequencies higher than 1100 cm^{-1}. On the basis of the calculations and analyses, normal mode assignments were made and mode symmetries determined.

I. Introduction

A good understanding of the microscopic physical and chemical processes that occur in shock wave initiation of condensed energetic materials is needed to address issues related to explosive sensitivity, safety, and performance. Because typical high explosives (HE) are organic molecular solids, the identity of the individual molecules as they exist in the liquid and gaseous state is preserved in the solid.[1] For shock compression to result in a chemical reaction, shock wave deformation of HE crystals must result in energy transfer to the internal degrees of freedom of the molecules. Although the energy transfer mechanisms have not been established, it is recognized that vibrational properties of both the crystal lattice and the individual molecule likely play an important role in this process.[2−6] Thus, there exists a need for detailed characterization of internal molecular vibrations. In the present work, we focus on the same for 1,3-propanediol, 2,2-bis(nitroxy)methyl-, dinitrate (ester), also known as pentaerythritol tetranitrate (PETN).

PETN is a crystalline energetic material used extensively as an initiating or booster high explosive. It was shown that the shock initiation of PETN depends strongly on the orientation of the crystal axes relative to the shock propagation direction.[7−9] A mechanistic understanding of this anisotropic behavior is an area of active interest.[10−12] High-resolution vibrational spectroscopy (IR and Raman) measurements under shock loading are needed to address questions related to anisotropic sensitivity and energy transfer. In the past, vibrational spectroscopy has been applied successfully to study various materials subjected to shock wave compression.[13−21] There have also been attempts to obtain vibrational spectra of PETN under shock wave and static high-pressure loading.[22,23] However, these attempts were hampered by experimental difficulties and by the lack of understanding of the complex structure of the PETN vibrational spectrum.

Unlike simpler molecules such as nitromethane, carbon tetrachloride, methyl nitrate, etc., it is difficult to make mode assignments in large polyatomic molecules, such as PETN, solely on the basis of characteristic group frequencies.[24,25] Usually, advanced electronic structure methods are needed for mode assignments. Recently, geometry optimizations and normal-mode analyses were reported for three conformers of 1,3,5-trinitro-*s*-triazine (RDX), a widely used, highly energetic molecule.[26,27] The results indicated that density functional theory (DFT) methods can be applied to large polyatomic, energetic molecules to obtain reliable results for molecular structure,[26,27] intramolecular force fields, and vibrational spectra.[26] Building on the conclusions of the RDX work, we applied DFT methods to PETN, which is similar in size to RDX.

As determined by X-ray diffraction measurements, the space group of the PETN crystal is $P\bar{4}2_1c$ and the molecular point group is S_4.[28,29] Hence, the PETN conformer belonging to the S_4 molecular point group comprises this molecular solid and a detailed study of this conformer is warranted. Our results for the S_4 conformer are reported in the present paper. The optimized molecular structure and vibrational spectra (Raman and IR) of this conformer were obtained using ab initio and DFT methods and are compared against the experimental data. Comprehensive analyses of several additional PETN conformers will be reported in the future.[30]

The remainder of this manuscript is organized as follows: the computational approach and experimental methods used are described briefly in the next section. Section III presents the calculated structure of the PETN molecule and its vibrational spectra; both the structure and spectra are compared with the experimental data. The results are summarized in section IV.

II. Approach and Methods

A. Computational Approach. All calculations were performed using the Gaussian 98 suite of quantum chemistry programs.[31] The molecule layout used in the calculations is shown in Figure 1. Second-order Moeller−Plesset (MP2)[32] and DFT (B3LYP[33,34] and B3PW91[34,35] hybrid functionals) geometry optimizations using the 6-31G(d) basis set[36−38] were carried out to determine the difference in theoretical treatments. Basis set effects were evaluated for the B3LYP density functional using the 6-31G(d) and 6-311+G(d,p)[39,40] basis sets. The DFT calculations employed the default grid provided in Gaussian 98

* Corresponding author. E-mail: shock@wsu.edu.

10.1021/jp004425j CCC: $20.00
Published on Web 05/25/2001

TABLE 1: Structural Parameters of PETN (S_4 Molecular Point Group)

parameter	MP2/6-31G(d)	B3PW91/6-31G(d)	B3LYP/6-31G(d)	B3LYP/6-311+G(d,p)	exptl meas[a,b]
			Bond Length, Å		
C1−C2	1.5309	1.5381	1.5438	1.5428	1.536
C2−O3	1.4419	1.4344	1.4422	1.4442	1.434
O3−N4	1.4377	1.4175	1.4314	1.4368	1.397
N4−O5	1.2208	1.2068	1.2113	1.2040	1.222
N4−O6	1.2160	1.1989	1.2030	1.1951	1.207
C2−H22	1.0934	1.0932	1.0923	1.0901	1.03
C2−H23	1.0931	1.0933	1.0924	1.0902	1.03
			Bond Angle, deg		
C2−C1−C7	108.74	108.71	108.70	108.63	109.2
C2−C1−C12	110.95	111.01	111.02	111.16	109.9
C1−C2−O3	105.21	106.38	106.36	106.29	107.5
C1−C2−H22	111.08	111.04	111.11	111.03	110.5
C1−C2−H23	110.67	110.42	110.49	110.43	110.0
H22−C2−H23	109.31	109.01	109.09	109.45	111.6
C2−O3−N4	112.65	113.67	113.70	114.19	115.9
O3−N4−O5	116.88	116.96	116.98	116.89	117.8
O3−N4−O6	111.98	112.36	112.28	112.30	113.3
O5−N4−O6	131.13	130.68	130.74	130.81	128.8

[a] Data of ref 28. [b] Typical standard deviations for bond lengths are ∼0.001 Å for the heavy atoms and ∼0.01 Å for the hydrogen atoms; bond angles are precise to within ∼0.1° and ∼1.0° for the bonds involving the heavy atoms only and at least one hydrogen atom, respectively.[28,29]

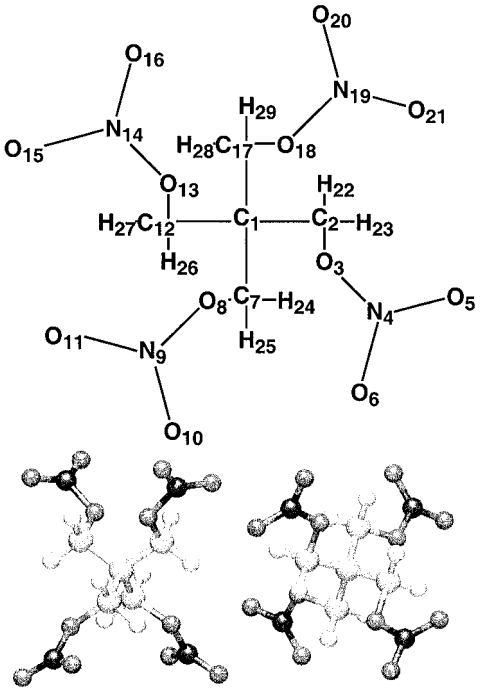

Figure 1. Molecular layout used in the calculations and ball-and-stick model for the S_4 conformer of PETN (two orthogonal projections are shown).

which was a pruned (75, 302) grid, having 75 radial shells and 302 angular points per shell.[31] "Tight" convergence criteria and analytical second derivatives were used in the calculations.

Normal-mode analyses were carried out for the optimized geometries, and the IR and Raman vibrational spectra were obtained for comparison with experiment. Spectral lines were simulated by fitting the predicted IR intensities/Raman activities to Lorentzian functions with the full width half-maximum (fwhm) arbitrarily set to 6 cm^{-1}. The Raman spectrum was simulated assuming a 514.5 nm excitation wavelength.[41] Atomic motions corresponding to each normal mode were determined using the MOLDEN interactive visualization and animation program.[42]

B. Experimental Methods. Thin rectangular slides (ca. 0.8 mm thick and 8 mm wide) of PETN single crystals were used to acquire Raman spectra. The Raman system consisted of a triple spectrometer (Spex 1877) equipped with a liquid nitrogen-cooled CCD detector (Princeton Instruments). The 514.5 nm line of a CW argon-ion laser was used as the excitation source. For IR absorption measurements, fine PETN powder was mixed with IR-grade KBr in 1:300 ratio by weight. The resulting mixture was pressed into pellets having the PETN area density of 2 mg/cm^2. The pellets were held under vacuum at room temperature and a Bomem-DA8 FTIR instrument was used for spectra acquisition.

III. Results and Discussion

A. Structural Data. Table 1 lists the geometric parameters of the S_4 conformer predicted using various theoretical methods along with parameters obtained from X-ray diffraction measurements of the PETN crystal.[28] Cartesian atomic coordinates of the optimized structures are given in Supporting Information Table 1S. The labeling of the atoms in Table 1 is consistent with the labeling in the molecular layout in Figure 1 and with the ball-and-stick model shown in the same figure. Of the four theoretical treatments, the B3PW91/6-31G(d) predictions have the smallest deviation from experimental measurements for the bond lengths, although differences for all four methods are small. Average absolute deviation of bond length predictions from experiments fall within 2.3−2.6% for various methods. The largest differences between theoretical predictions and the experimental data are for the C−H bonds; all methods systematically overestimate the C−H bond lengths by ∼6%.

In agreement with experiments, all methods predict a slight distortion from the tetrahedral coordination for the central carbon. However, the experimental magnitude of this distortion (∼0.4°) is appreciably smaller than the calculated value of ∼1.5°. As expected, the four atoms comprising the nitrate group are truly planar, as verified by the sum of the O−N−O angles, which equals 360° for all methods. The calculations also indicate that the carbon atom adjacent to the ONO_2 group, the central carbon, and a C−H group of the neighboring $-CH_2ONO_2$ arm lie nearly perfectly in the corresponding ONO_2 plane. For example, calculations predict that the H28−C17−C1−C2−O3−N4−O5−O6 group of atoms forms a single plane to within dihedral distortions no greater than ∼1.5°. There are four such planes in the molecule that form a dihedral angle of ∼120° with

TABLE 2: Vibrational Frequencies of PETN (S_4 Molecular Point Group)[a]

	B3LYP/6-31G(d)				B3LYP/6-311+G(d,p)					experiment [b]		
no.	freq	IR int	Raman act.	irr rep	freq	IR int	Raman act.	irr rep	assignment [c,d]	IR [e]	IR [f]	Raman [f]
1	24	0	2.5	A	23	2	1.5	B	O′−N b + C_5 skl			
2	26	2	1.3	B	24	0	2.9	A	O′−N b			
3	39	2	1.1	E	37	2	1.5	E	NO wag + C_5 skl			
4	40	0	2.5	B	38	0	3.1	B	ONO_2 wag			
5	50	0	0.7	A	45	0	0.9	A	O′−N t			
6	51	0	0.6	B	50	0	0.7	B	ONO_2 r			
7	56	3	2.2	E	53	4	2.2	E	O′−N t + C_5 skl			
8	125	1	0.1	E	119	2	0.2	E	C−CO wag			
9	139	1	1.0	B	130	2	1.2	B	CC t			
10	150	0	4.0	A	144	0	4.2	A	C−O↑−N wag			
11	173	0	0.3	A	168	0	0.5	A	$CONO_2$ r			
12	195	2	0.9	E	191	2	0.8	E	O−CH_2 t + CCC def			
13	212	0	6.1	A	208	0	8.0	A	$CONO_2$ r			
14	251	2	1.4	B	248	2	1.4	B	ONO_2 r + C_5 skl			
15	254	5	3.7	E	251	3	4.3	E	CH_2 r + ONO_2 r + C_5 skl			
16	311	2	0.5	B	307	1	0.6	B	CH_2 r + CCC def			
17	319	0	0.3	A	316	0	0.2	A	CH_2 r			319w
18	453	7	4.2	E	447	9	4.2	E	CCC def + O′−N st + NO_2 r		460w	459m
19	536	11	9.5	B	525	25	8.2	B	C_5 skl + CH_2 wag + O′−N st			539w
20	585	0	7.6	A	586	0	8.6	A	CC b + ONO_2 r			589s
21	617	9	5.2	B	618	13	5.2	B	C_5 skl + ONO_2 r	619w	618w	619sh
22	623	14	27.1	E	620	28	28.8	E	CCC def + ONO_2 r	623w	624m	624s
23	673	0	15.4	A	670	0	21.6	A	O′−N st + CC st + NO_2 sc			676m
24	710	87	6.7	E	704	171	9.2	E	O′−N st + CCC def + NO_2 r	703m	704s	704m
25	753	8	2.8	B	751	95	4.8	B	CCC def + O′−N st	746w	746m	746w
26	756	30	0.0	E	761	24	0.1	E	ONO_2 umb			
27	757	0	0.7	A	761	0	0.3	A	ONO_2 umb			
28	760	61	1.9	B	763	57	1.1	B	ONO_2 umb + CCC def	754m	755s	755w
29	842	0	3.6	A	839	0	2.4	A	CC st			839m
30	855	758	24.1	E	843	762	25.5	E	O′−N st	851m	852s	854m
31	860	753	1.4	B	845	778	3.0	B	O′−N st	870m	869s	869sh
32	886	0	69.9	A	873	0	80.6	A	O′−N st + CC st			873s
33	934	9	7.5	B	918	7	5.1	B	CCC def + CH_2 r			900sh
34	952	14	4.0	E	941	15	2.6	E	CH_2 t + CCC def	939w	939w	939w
35	1023	0	0.8	A	1006	0	0.3	A	CH_2 r + CO st			995sh
36	1038	156	1.7	E	1019	133	2.2	E	CO st + CCC def	1003m	1003m	1004w
37	1071	0	4.1	A	1055	0	4.1	A	CH_2 t + CC b			1044m
38	1074	120	5.3	B	1058	108	5.1	B	CO st + C_5 skl + NO_2 r	1038m	1038m	1037sh
39	1194	3	1.3	B	1176	2	1.5	B	CH_2 wag + C_5 skl		1159vw	
40	1212	1	5.0	E	1199	0	6.5	E	CCC def + CH_2 wag		1193vw	1195m
41	1274	0	25.8	A	1265	0	15.6	A	CH b			1253s
42	1295	49	5.5	E	1284	56	3.9	E	CH b + C_5 skl		1257vw	
43	1319	275	5.3	B	1306	370	3.4	B	CH b + C_5 skl + ONO_2 r	1271s	1272vs	1273w
44	1336	580	7.0	E	1318	599	10.5	E	NO_2 st (s) + CH b + C_5 skl	1284s	1285vs	1286sh
45	1351	0	7.9	A	1331	0	18.0	A	NO_2 st (s) + CH_2 wag			1294vs
46	1352	212	1.8	B	1335	150	2.1	B	CH_2 wag + C_5 skl + NO_2 r	1306m	1306m	
47	1417	78	1.7	E	1404	56	0.4	E	CH_2 wag + CCC def	1385w	1387m	
48	1422	56	2.0	B	1408	43	1.1	B	CH_2 wag + CCC def	1396w	1396m	1397sh
49	1435	0	9.5	A	1423	0	9.5	A	CH_2 wag + CC st (s)			1406m
50	1535	0	3.4	A	1513	0	2.0	A	CH_2 sc			
51	1536	4	18.5	B	1513	5	11.4	B	CH_2 sc		1509vw	1512m
52	1541	27	1.6	E	1520	32	0.8	E	CH_2 sc	1474w	1474m	1474m
53	1775	0	0.7	A	1731	0	1.8	A	NO_2 st (a)			1633m
54	1776	220	4.6	B	1732	276	8.6	B	NO_2 st (a)	1655s	1661s	1665s
55	1778	1083	5.4	E	1734	1401	10.8	E	NO_2 st (a)	1645vs	1648vs	1650w
56	3102	6	0.1	B	3077	7	0.3	B	CH_2 st (s)			
57	3103	13	17.7	E	3078	11	6.5	E	CH_2 st (s)			2940w
58	3105	0	251.1	A	3080	0	329.4	A	CH_2 st (s)	2984vw	2985vw	2987vs
59	3159	0	0.1	A	3134	0	0.1	A	CH_2 st (a)			
60	3161	13	72.9	E	3136	9	64.4	E	CH_2 st (a)	3023vw	3023w	3025s
61	3163	13	49.9	B	3138	7	43.6	B	CH_2 st (a)	2910vw	2916w	2918s

[a] Frequency in cm^{-1} (nonscaled frequencies are given); IR intensities and Raman activities in km/mol and $Å^4$/amu, respectively; combined intensity/activity is given for the doubly degenerate E vibrations. [b] vw = very weak, w = weak, m = medium, s = strong, vs = very strong, sh = shoulder. [c] st = stretch, b = bend, sc = scissors, umb = umbrella, skl = skeletal, t = torsion, def = deformation, r = rock, (a) = antisymmetric, (s) = symmetric, O′ = ester oxygen. [d] Assignments are given based on the B3LYP/6-311+G(d,p) calculation; the most prominent contribution to each mode is listed first. [e] Reference 23. [f] This work.

one another. Average angle deviations from experimental data are ca. 1% with the MP2/6-31G(d) results being the least accurate and the B3LYP/6-311+G(d,p) results being the most accurate (average deviations of 1.3% and 1.0%, respectively).

The overall good agreement in the calculated and measured geometries is remarkable since the experimental information was obtained for molecules in the solid state while the theoretical calculations were performed for a single PETN molecule. Hence,

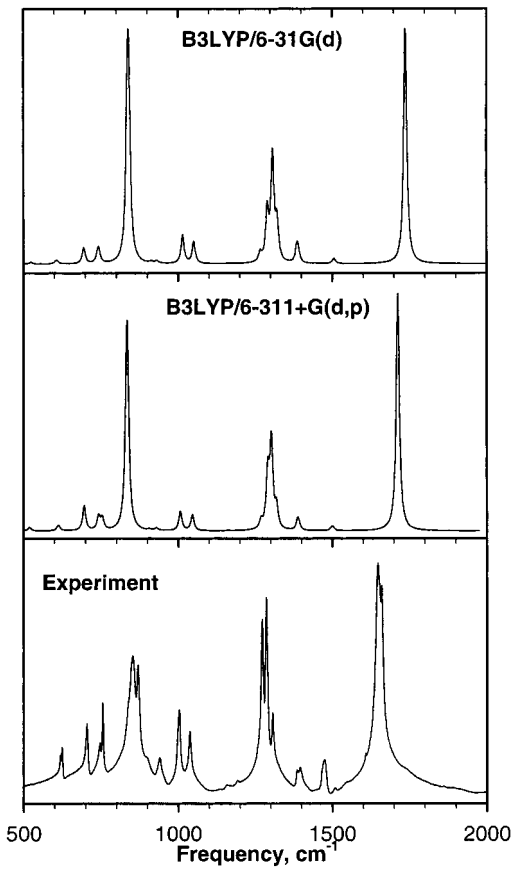

Figure 2. Simulated infrared absorption spectra of PETN at the B3LYP/6-31G(d) (top panel) and B3LYP/6-311+G(d,p) (middle panel) levels of theory. As discussed in the text, the vibrational frequencies used to generate these spectra are reduced by 2.26% and 1.24%, respectively. The bottom panel displays the experimental spectrum obtained in our work.

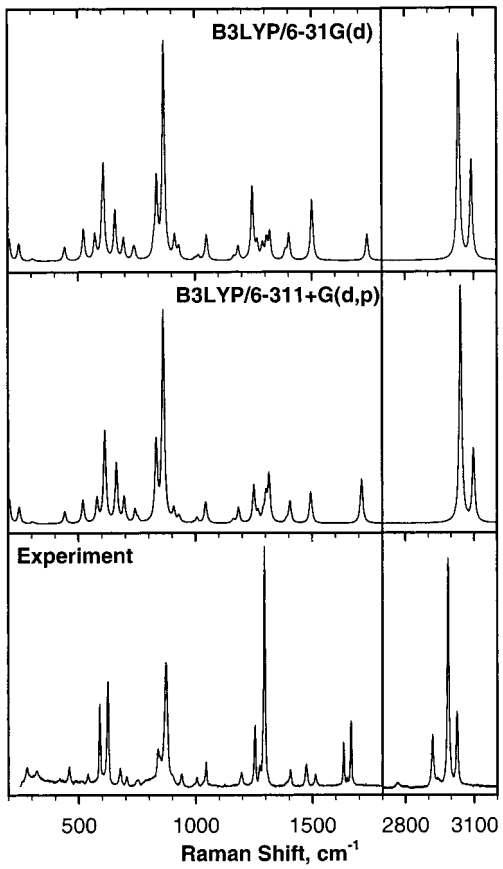

Figure 3. Simulated Raman spectra of PETN at the B3LYP/6-31G(d) (top panel) and B3LYP/6-311+G(d,p) (middle panel) levels of theory. As discussed in the text, the vibrational frequencies used to generate these spectra are reduced by 2.26% and 1.24%, respectively. The bottom panel displays the experimental spectrum obtained in our work. The vertical solid line denotes a break in the spectra; there are no Raman bands in the omitted spectral region from 1800 to 2700 cm^{-1}.

the crystal field does not seem to significantly distort the molecule. Among the methods used, the ab initio treatment (MP2) appears to be the least accurate; all of the DFT treatments produce very comparable results.

B. Vibrational Spectra. The 81 internal vibrational modes of PETN (Γ_g) belong to the following irreducible representations of the S_4 molecular point group: $\Gamma_g = 20A + 21B + 20E$. The 20 A modes are not IR active and the 20 E modes are doubly degenerate.[43] Table 2 provides the calculated vibrational frequencies for the B3LYP/6-31G(d) and B3LYP/6-311+G(d,p) calculations, the corresponding IR intensities (km/mol) and Raman activities (Å^4/amu), and symmetry assignments. The B3LYP/6-311+G(d,p) results also include assignments of atomic motions corresponding to each normal mode.

Experimental IR and Raman spectra of PETN available in the literature were obtained primarily for the purpose of trace explosives detection and forensic studies.[44−49] The information provided in these publications was mostly qualitative, and accurate frequencies and line widths were not given. One exception was ref 23 where the IR frequencies were partially tabulated. To accurately compare the calculated frequencies with experimental data, we measured both Raman and IR spectra of PETN, as described in section IIB. The results are summarized in Table 2 and the spectra are shown in Figures 2 and 3. The availability of both IR and Raman spectra enabled us to assign unambiguously the measured vibrational bands to their theoretical counterparts despite some mismatch in the frequency values. This assignment is also presented in Table 2.

Simulated spectra obtained using the B3LYP calculations are compared against the experimental spectra in Figures 2 and 3. The vibrational frequencies in these figures were reduced by 2.26 and 1.24% for the B3LYP/6-31G(d) and B3LYP/6-311+G(d,p) results, respectively. These scaling factors were chosen to minimize the sum of weighted square deviations between the theoretical and experimental frequencies.[50] The overall scaling of the B3LYP/6-311+G(d,p) spectra is slightly better than that of the B3LYP/6-31G(d), as it results in smaller σ [2]. Results of the B3PW91/6-31G(d) calculation (not shown) were very similar to the B3LYP/6-31G(d) spectra. In agreement with the trend indicated in ref 26, the MP2/6-31G(d) results (also not shown) were in poorest agreement with experimental data.

As can be seen in Figures 2 and 3, all of the major features of the PETN vibrational spectra are reproduced very well and the region below 1100 cm^{-1} is modeled remarkably well. However, there are several discrepancies between the theoretical and experimental spectra above 1100 cm^{-1}. In particular, the calculations fail to reproduce the high intensity of the 1294 cm^{-1} Raman band assigned in the literature[25] to the NO_2 symmetric stretch. As suggested by the basis set effect (see Table 2), the reason for this could lie in the mixing of the two strong bands located experimentally at 1253 and 1294 cm^{-1}. These two bands can mix in the calculation because both are of A symmetry. In the 6-31G(d) calculation, the 1253 cm^{-1} band identified as a CH bending mode appears to be of higher intensity than the 1294 cm^{-1} mode. The order is reversed in the 6-311+G(d,p)

calculation. The latter ordering agrees with experimental data (see Figure 3).

Another apparent problem is that some of the experimentally resolved vibrational bands appear overlapped in the calculated spectra. In particular, the three NO_2 antisymmetric stretching modes located around 1650 cm^{-1} are fully resolved in the Raman spectrum (see Figure 3) and are partially resolved in the IR spectrum (see Figure 2). However, the calculated frequencies for these modes lie within 3 cm^{-1} of one another and, consequently, these modes form a single band in the simulated spectra; recall that the calculations had a fwhm of 6 cm^{-1}. In the 3000 cm^{-1} range, the calculation correctly predicts the three strong Raman peaks associated with CH_2 stretching modes. However, the two antisymmetric stretching modes appear superimposed in the simulation while they are well apart in the experimental spectrum. At this point it is not clear whether these effects are due to the crystal field or are an artifact of the calculation.

From the mode assignments given in Table 2, it becomes immediately apparent that very few normal modes represent "pure" motion of specific functional groups within the PETN molecule, as is often the case for smaller molecules.[25] Instead, various normal modes involve contributions from the motion of many functional groups. A good illustration of this behavior is the strong IR mode at 1285 cm^{-1} previously assigned to the NO_2 symmetric stretch.[23] We find that in addition to the NO_2 stretching motion this mode contains significant contributions from a CH bend and C_5 skeletal deformation. Atomic displacements for each normal mode can be obtained from the authors upon request.

In classifying the normal modes in Table 2, we used the following convention: in-plane symmetric bending modes were denoted as scissors; other in-plane vibrations that involved three or more atoms of a planar group were denoted as rocking modes. Wagging modes were defined as out-of-plane vibrations; one exception was the ONO_2 umbrella motion that involved an out-of-plane vibration of the nitrogen accompanied by the counterphase motion of the oxygen atoms. Three types of carbon backbone vibrations were differentiated. The modes that included large vibrations of the quaternary carbon and relatively small vibrations of the secondary carbons were denoted as CCC deformations. When vibrational amplitudes of all five carbons were comparable, the corresponding modes were denoted as C_5 skeletal vibrations. When the quaternary carbon remained stationary with only the secondary carbons moving, such modes were designated as CC stretching or bending modes. Finally, the designation of bending, stretching, and torsional modes adhered to the textbook definitions.[41]

IV. Summary

Geometry optimizations and normal-mode analyses of the PETN conformer belonging to the S_4 molecular point group have been performed using ab initio (MP2) and DFT (B3LYP and B3PW91) methods. The basis sets used in this study were 6-31G(d) and 6-311+G(d,p). The structural results are in good agreement with experimental X-ray diffraction data. The predicted bond lengths and bond angles are accurate to within ~2.5% and ~1.2%, respectively. Raman and IR spectra of crystalline PETN have been measured and compared with the simulated spectra. The two sets of spectra agree very well in the spectral region below 1100 cm^{-1}; the agreement is satisfactory for frequencies higher than 1100 cm^{-1}. In particular, the calculations do not reproduce well the high intensity of the 1294 cm^{-1} Raman band. Also, three NO_2 antisymmetric stretching modes and two CH_2 antisymmetric stretching modes located around 1650 and 3000 cm^{-1}, respectively, appear superimposed in the calculations while they are well resolved experimentally. No definite conclusion could be reached as to whether this is due to a crystal field effect or is an artifact of the calculation. On the basis of the calculations and analyses, normal mode assignments have been made and mode symmetries determined. The overall good agreement between calculated and measured geometry and vibrational spectra is remarkable since the experimental data were obtained for crystalline PETN and the calculations were performed for a single PETN molecule. In general, the MP2 results are in poorer agreement with experimental data while all of the DFT methods used produce very good results.

Acknowledgment. All calculations were performed on the HP/Convex Exemplar SPP-2000 supercomputer at the National Center for Supercomputing Applications (NCSA) of the University of Illinois at Urbana—Champaign. We gratefully acknowledge the NCSA for the allotment of computer time under grant DMR990014N. We also thank Dr. J. J. Dick for providing PETN samples, Prof. M. D. McCluskey for access to the FTIR instrument, and Prof. R. D. Poshusta for valuable suggestions. This work was supported by ONR grant N000149911014 and DOE grant DEFG0397SF21388.

Supporting Information Available: Atomic coordinates for the optimized structures of PETN. This material is available free of charge via the Internet at http://pubs.acs.org.

References and Notes

(1) Galwey, A. K. *Chemistry of Solids*; Chapman and Hall: London, 1967.
(2) Dlott, D. D.; Fayer, M. D. *J. Chem. Phys.* **1990**, *92*, 3798.
(3) Tokmakoff, A.; Fayer, M. D.; Dlott, D. D. *J. Phys. Chem.* **1993**, *97*, 1901.
(4) Coffey, C. S.; Toton, E. T. *J. Chem. Phys.* **1982**, *76*, 949.
(5) Bardo, R. D. *Int. J. Quantum Chem. Symp.* **1986**, *20*, 455.
(6) Tarver, C. M. *J. Phys. Chem. A*, **1997**, *101*, 4845.
(7) Dick, J. J. *Appl. Phys. Lett.* **1984**, *44*, 859.
(8) Dick, J. J.; Mulford, R. N.; Spencer, W. J.; Pettit, D. R.; Garcia, E.; Shaw, D. C. *J. Appl. Phys.* **1991**, *70*, 3572.
(9) Yoo, C. S.; Holmes, N. C.; Souers, P. C.; Wu, C. J.; Ree, F. H.; Dick, J. J. *J. Appl. Phys.* **2000**, *88*, 70.
(10) Dick, J. J.; Ritchie, J. P. *J. Appl. Phys.* **1994**, *76*, 2726.
(11) Jindal, V. K.; Dlott, D. D. *J. Appl. Phys.* **1998**, *83*, 5203.
(12) Gruzdkov, Y. A.; Gupta, Y. M. *J. Phys. Chem. A* **2000**, *104*, 11169.
(13) Dlott, D. D. *Annu. Rev. Phys. Chem.* **1999**, *50*, 251.
(14) Yoo, C. S.; Gupta, Y. M.; Horn, P. D. *Chem. Phys. Lett.* **1989**, *159*, 178.
(15) Pangilinan, G. I.; Gupta, Y. M. *J. Phys. Chem.* **1994**, *98*, 4522.
(16) Pangilinan, G. I.; Gupta, Y. M. *J. Appl. Phys.* **1997**, *81*, 6662.
(17) Winey, J. M.; Gupta, Y. M. *J. Phys. Chem. B* **1997**, *101*, 10733.
(18) Gupta, Y. M.; Gruzdkov, Y. A.; Pangilinan, G. I. *Chem. Phys. Lett.* **1998**, *283*, 251.
(19) Hare, D. E.; Franken, J.; Dlott, D. D. *Chem. Phys. Lett.* **1995**, *244*, 224.
(20) Hare, D. E.; Franken, J.; Dlott, D. D. *J. Appl. Phys.* **1995**, *77*, 5950.
(21) Hambir, S. A.; Franken, J.; Hare, D. E.; Chronister, E. L.; Baer, B. J.; Dlott, D. D. *J. Appl. Phys.* **1997**, *81*, 2157.
(22) Trott, W. M.; Renlund, A. M. *Appl. Opt.* **1985**, *24*, 1520.
(23) Foltz, M. F. *Proc. 10th Symp. (Int.) Detonation* **1993**, 579.
(24) Szymanski, H. A. *Correlation of Infrared and Raman Spectra of Organic Compounds*; Hertillon Press: Cambridge Springs, PA, 1969.
(25) Dollish, F. R.; Fateley, W. G.; Bentley, F. F. *Characteristic Raman Frequencies of Organic Compounds*; Wiley: New York, 1974.
(26) Rice, B. M.; Chabalowski, C. F. *J. Phys. Chem. A* **1997**, *101*, 8720.
(27) Harris, N. J.; Lammertsma, K. *J. Am. Chem. Soc.* **1997**, *119*, 6583.
(28) Cady, H. H.; Larson, A. C. *Acta Crystallogr.* **1975**, *B31*, 1864.
(29) Conant, J. W.; Cady, H. H.; Ryan, R. R.; Yarnell, J. L.; Newsam, J. M. *Informal Report LA-7756-MS*; Los Alamos National Laboratory: Los Alamos, NM, 1979.
(30) Gruzdkov, Y. A.; Dreger, Z. A.; Gupta, Y. M. *J. Phys. Chem. A*, in preparation.

(31) Frisch, M. J.; Trucks, G. W.; Schlegel, H. B.; Scuseria, G. E.; Robb, M. A.; Cheeseman, J. R.; Zakrzewski, V. G.; Montgomery, J. A., Jr.; Stratmann, R. E.; Burant, J. C.; Dapprich, S.; Millam, J. M.; Daniels, A. D.; Kudin, K. N.; Strain, M. C.; Farkas, O.; Tomasi, J.; Barone, V.; Cossi, M.; Cammi, R.; Mennucci, B.; Pomelli, C.; Adamo, C.; Clifford, S.; Ochterski, J.; Petersson, G. A.; Ayala, P. Y.; Cui, Q.; Morokuma, K.; Malick, D. K.; Rabuck, A. D.; Raghavachari, K.; Foresman, J. B.; Cioslowski, J.; Ortiz, J. V.; Baboul, A. G.; Stefanov, B. B.; Liu, G.; Liashenko, A.; Piskorz, P.; Komaromi, I.; Gomperts, R.; Martin, R. L.; Fox, D. J.; Keith, T.; Al-Laham, M. A.; Peng, C. Y.; Nanayakkara, A.; Gonzalez, C.; Challacombe, M.; Gill, P. M. W.; Johnson, B.; Chen, W.; Wong, M. W.; Andres, J. L.; Gonzalez, C.; Head-Gordon, M.; Replogle, E. S.; Pople, J. A. *Gaussian 98*, revision A.7; Gaussian, Inc.: Pittsburgh, PA, 1998.

(32) Moeller, C.; Plesset, M. S. *Phys. Rev. A* **1934**, *46*, 618.

(33) Becke, A. D. *J. Chem. Phys.* **1993**, *98*, 5648.

(34) Lee, C.; Yang, W.; Parr, R. G. *Phys. Rev. B* **1988**, *37*, 785.

(35) Burke, K.; Perdew, J. P.; Wang, Y. In *Electronic Density Functional Theory: Recent Progress and New Directions*; Dobson, J. F., Vignale, G., Das, M. P., Eds.; Plenum Press: London, 1998.

(36) Hehre, W. J.; Ditchfield, R.; Pople, J. A. *J. Chem. Phys.* **1972**, *56*, 2257.

(37) Hariharan, P. C.; Pople, J. A. *Theor. Chim. Acta* **1973**, *28*, 213.

(38) Gordon, M. S. *Chem. Phys. Lett.* **1980**, *76*, 163.

(39) McLean, A. D.; Chandler, G. S. *J. Chem. Phys.* **1980**, *72*, 5639.

(40) Krishnan, R.; Binkley, J. S.; Seeger, R.; Pople, J. A. *J. Chem. Phys.* **1980**, *72*, 650.

(41) Wilson, E. B., Jr.; Decius, J. C.; Cross, P. C. *Molecular Vibrations: The Theory of Infrared and Raman Vibrational Spectra*; Dover Publications: New York, 1955.

(42) http://www.cmbi.kun.nl/~schaft/molden/molden.html.

(43) Cotton, F. A. *Chemical Applications of Group Theory*; Wiley: New York, 1990.

(44) Pristera, F.; Halik, M.; Castelli, A.; Fredericks, W. *Anal. Chem.* **1960**, *32*, 495.

(45) Carol, J. *J. Assoc. Offic. Agricul. Chem.* **1960**, *43*, 259.

(46) Akhavan, J. *Spectrochim. Acta* **1991**, *47A*, 1247.

(47) Munro, C.; Pajcini, V.; Asher, S. A. *Appl. Spectrosc.* **1997**, *51*, 1722.

(48) Lewis, I. R.; Daniel, N. W., Jr.; Griffiths, P. R. *Appl. Spectrosc.* **1997**, *51*, 1854.

(49) Janni, J.; Gilbert, B. D.; Field, R. W.; Steinfield, J. I. *Spectrochim. Acta A* **1997**, *53*, 1375.

(50) To obtain scaling factor α the following function was minimized: $\sigma^2 = (1/N)\sum_{i=1}^{N}(\alpha\omega_i^c - \omega_i^e)^2/(\omega_i^e)^2$, where ω_i^e and ω_i^c are experimental and calculated frequencies, respectively.